

Thermally Induced Crossover from 2D to 1D Behavior in an Array of Atomic Wires: Silicon Dangling-Bond Solitons in Si(553)-Au

B. Hafke^{1,*}, C. Brand¹, T. Witte¹, B. Sothmann¹, M. Horn-von Hoegen¹, and S. C. Erwin²

¹Faculty of Physics and Center for Nanointegration (CENIDE), University of Duisburg-Essen, 47057 Duisburg, Germany

²Center for Computational Materials Science, Naval Research Laboratory, Washington, D.C. 20375, USA



(Received 12 April 2019; published 10 January 2020)

The self-assembly of submonolayer amounts of Au on the densely stepped Si(553) surface creates an array of closely spaced “atomic wires” separated by 1.5 nm. At low temperature, charge transfer between the terraces and the row of silicon dangling bonds at the step edges leads to a charge-ordered state within the row of dangling bonds with $\times 3$ periodicity. Interactions between the dangling bonds lead to their ordering into a fully two-dimensional (2D) array with centered registry between adjacent steps. We show that as the temperature is raised, soliton defects are created within each step edge. The concentration of solitons rises with increasing temperature and eventually destroys the 2D order by decoupling the step edges, reducing the effective dimensionality of the system to 1D. This crossover from higher to lower dimensionality is unexpected and, indeed, opposite to the behavior in other systems.

DOI: [10.1103/PhysRevLett.124.016102](https://doi.org/10.1103/PhysRevLett.124.016102)

Physical phenomena associated with low dimensionality are suppressed when the temperature is raised. For example, the 2D fractional quantum Hall effect [1,2] and the 1D Tomonaga-Luttinger liquid [3–5] are observed only at low temperature. In 1D atomic wire systems at low temperatures, Peierls distortions or more general symmetry breakings can open a gap at the Fermi level and lower the total energy by forming a charge density wave [6–8] or spin-density wave [9–12].

Excitations generally wash out the effects of this anisotropy and hence suppress low-dimensional behavior. The resulting crossover to higher dimensionality at increased temperatures is exhibited by many systems. Recent examples include the atomic wire systems Pt (110)-Br and Si(557)-Pb. In these systems, structural changes are accompanied by a delicate interplay between charge density wave correlations and short-range interactions of the adsorbate atoms [13] and by correlated spin-orbit order that triggers a metal-to-insulator transition, respectively [14–17]. The resulting dimensional crossover from 1D to 2D is typical for atomic wire systems.

In this Letter, we demonstrate the opposite case: a system of coupled atomic wires exhibiting 2D order at low temperatures in which thermal excitations at higher temperatures induce a dimensional crossover to 1D behavior. We identify the mechanism driving this crossover to be the creation of phase solitons and antisolitons [18,19], which leads to a reversible order-disorder transition at higher temperatures [20]. We track the crossover across its characteristic temperature (approximately 100 K) using a combination of a quantitative high resolution spot profile analyzing low-energy electron diffraction (SPA-LEED) study, density-functional theory (DFT) calculations,

Monte Carlo statistical simulations, and an exactly solvable analytical model.

We studied the self-organized Si(553)-Au atomic wire surface consisting of Au double-atom rows on (111)-oriented Si terraces separated by bilayer steps [Fig. 1].

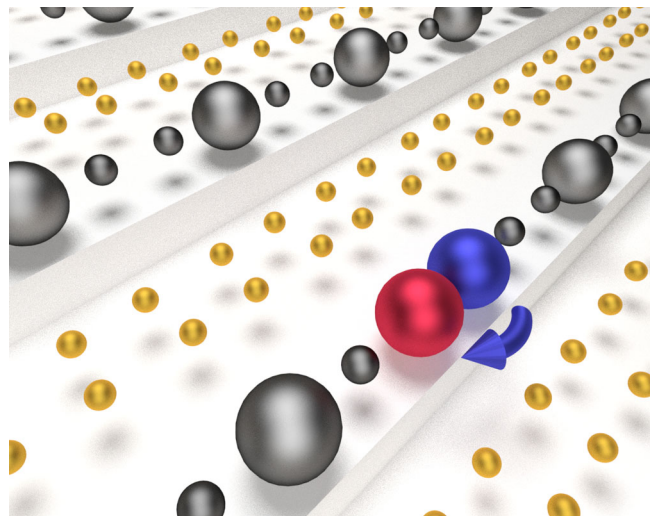


FIG. 1. Ground-state structure and low-energy excitation of the Si(553)-Au atomic wire system. The underlying substrate consists of Si(111) terraces separated by steps. Each terrace contains a dimerized double row of Au atoms (gold) and a row of Si dangling bonds (gray spheres) at the step edge. The electron occupancy of these dangling bonds creates a ground state with tripled periodicity: for every two saturated dangling bonds (SDBs, small spheres) there is a third, unsaturated dangling bond (UDB, large spheres). At finite temperatures, some of these UDBs (blue) become mobile and hop to adjacent sites (red). This excitation creates a soliton-antisoliton pair that can subsequently dissociate.

Charge transfer from the terraces leads to incomplete filling of the dangling sp^3 orbitals at the Si step edge [20–22]. The low-temperature ground state consists of a charge-ordered state with $\times 3$ periodicity along the step edges, which is observed in scanning tunneling microscopy (STM) [20,22–29] and LEED experiments [20,28–31]. The $\times 3$ periodicity along the wires represents the simplest way to distribute the available electrons among the row of dangling bonds while maximizing the number of fully saturated dangling bonds (electron lone pairs) [32]. Angle-resolved photoemission spectroscopy measurements [21,24,30,33] and DFT calculations [24,33–35] reveal that the dangling-bond states do not cross the Fermi level. Hence, all the dangling-bond orbitals have integer electron occupancies of 0, 1, or 2. We will refer to orbitals with occupancy 2 as saturated dangling bonds (SDBs) and to those less than 2 as unsaturated dangling bonds (UDBs). Figure 1 depicts the arrangement of UDBs and SDBs schematically. The ordering of the Si dangling-bond structure is mediated by Coulomb interaction of the UDBs (large spheres) with approximately equal spacing within and across the rows. The SDBs merely provide a compensating background charge to balance the reduced electron occupancy of the UDBs.

The actual number of electrons in the UDBs has been previously investigated using DFT. The result is sensitive to the choice of the exchange-correlation functional. The original prediction [34], which used the functional of Perdew, Burke, and Ernzerhof (PBE) [36], was that five electrons are shared among three dangling bonds with an electron configuration (2,2,1) having $\times 3$ periodicity and one unpaired spin [28]. More recent work [37], based on the revised PBEsol functional [38], predicted that only four electrons are shared among three dangling bonds, implying the configuration (2,2,0) with no unpaired spins. At present it is not possible to distinguish between these scenarios on the basis of experimental data. Here, we consider both possibilities and show that they lead to very different estimates of the order-disorder transition temperature.

The experiment was performed under ultrahigh vacuum conditions at a base pressure lower than 1×10^{-10} mbar. The Si substrate was cut from an n -type Si(553) wafer (phosphorus doped, $0.01 \Omega \text{ cm}$). Prior to Au deposition, the sample was cleaned in several short flash-anneal cycles by heating via direct current to 1250°C . Next, 0.48 ML [monolayer, referred to the atomic density of a Si(111) surface, i.e., $1 \text{ ML} = 7.83 \times 10^{14} \text{ atoms per cm}^2$] Au was deposited from an electron-beam-heated graphite crucible [39] at a substrate temperature of 650°C , followed by a postannealing step at 850°C for several seconds [25] and subsequent cooling to 60 K on a liquid helium cryostat. The temperature was measured by an Ohmic sensor (Pt100) directly clamped to the back of the sample.

At 60 K , the SPA-LEED pattern [Fig. 2(a)] reveals spots at $\times 3$ positions and streaks at $\times 2$ positions in the $[\bar{1}\bar{1}0]$ direction. The latter indicates the formation of Au atomic

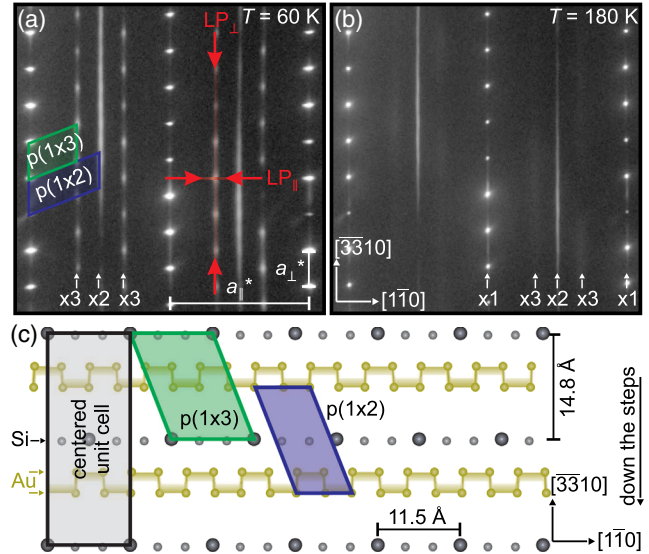


FIG. 2. SPA-LEED pattern of Si(553)-Au at an electron energy of 150 eV and temperatures (a) 60 K and (b) 180 K . The $\times 2$ streaks between the rows of sharp integer-order spots arise from dimerized Au double rows on the (111) -oriented terraces. The rows of elongated spots at $\times 3$ positions indicate the tripled periodicity and long-range order of the UDBs at the Si step edge. The intensity of the $\times 2$ streak is nearly unaffected at higher temperature, while the $\times 3$ features fade away. In (a) the unit cells of the Au (blue) and Si (green) sublattices as well as the directions of the line profiles LP_{\parallel} and LP_{\perp} (Fig. 3) are indicated (for more details see [28]). (c) Surface structural model showing Si step-edge atoms (gray) and Au atoms (gold). The unit cells are depicted with the same color coding as in (a).

wires. The spacing of the $\times 1$ spots corresponds to the reciprocal lattice constant $a_{\parallel}^* = 2\pi/(3.84 \text{ \AA})$ of the Si substrate along the steps. The $\times 3$ spots arise from ordering of the UDBs within the rows; hence, the UDBs have an intrarow separation of $3 \times a_{\parallel} = 11.5 \text{ \AA}$. The UDBs in different rows are in registry: recent investigations by SPA-LEED and STM reveal a centered $p(1 \times 3)$ arrangement [Figs. 2(a) and 2(c)] [28]. In the $[\bar{3}\bar{3}10]$ direction the reciprocal step-to-step distance is $a_{\perp}^* = 2\pi/(14.8 \text{ \AA})$ [21] and thus the separation between the UDB rows is 14.8 \AA . Hence, at low temperatures the UDBs in Si(553)-Au are arranged in rows in a fully ordered 2D array with approximately equal spacing within (11.5 \AA) and across (14.8 \AA) the rows. The $\times 2$ streaks are attributed to the dimerized double row of Au atoms on the (111) terrace of the surface [gold spheres in Fig. 2(c); the unit cell is shown by the blue-shaded areas in Figs. 2(a) and 2(c)] [35,40]. We did not detect any $\times 6$ periodicity in the $[\bar{1}\bar{1}0]$ direction, indicating that the Au atoms and Si step-edge atoms are structurally decoupled [27,28,31,37].

At 180 K , the intensity of the $\times 3$ spots fades markedly [Fig. 2(b)], in agreement with an earlier study [20], while the intensity of the $\times 2$ streaks is nearly unaffected.

To analyze the evolution of the diffraction pattern between 60 to 190 K (heating rate 0.13 K/s), we recorded a series of line profiles [Figs. 3(a) and 3(b)] through the $\times 3$ spots, in two orthogonal directions: $[\bar{3}\bar{3}10]$ (LP_{\perp} , across the steps) and $[1\bar{1}0]$ (LP_{\parallel} , along the steps). The $\times 3$ diffraction spots [insets of Figs. 3(a) and 3(b)] of each of the line profiles

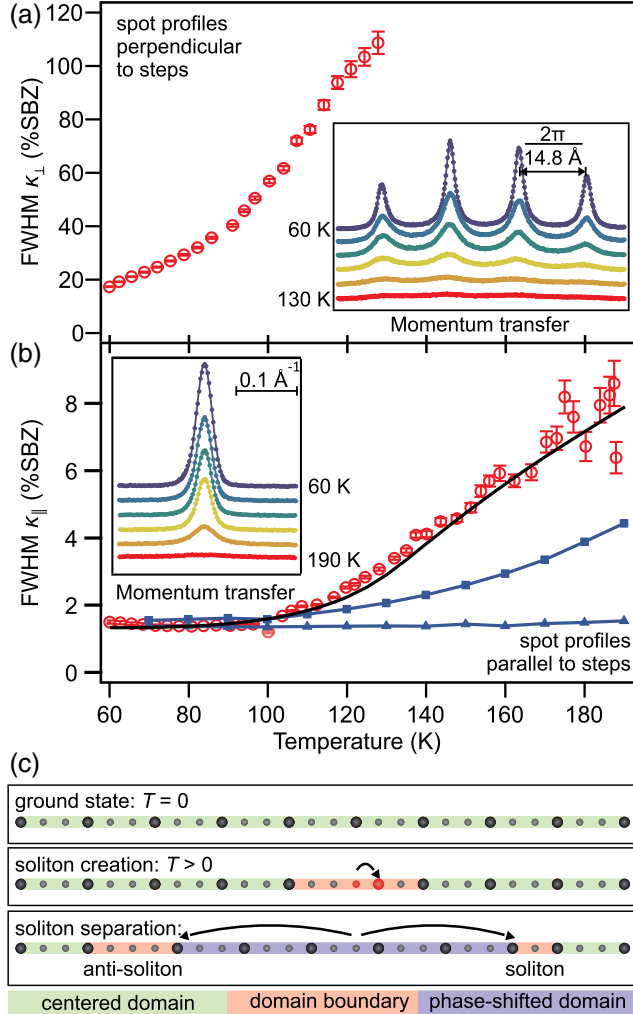


FIG. 3. FWHM of the $\times 3$ diffraction spots (red data points) as a function of temperature in (a) the $[\bar{3}\bar{3}10]$ direction and (b) the $[1\bar{1}0]$ direction, as indicated in Fig. 2(a). Results from Monte Carlo simulations based on DFT interactions are shown in (b) by blue squares for the (2,2,1) configuration and triangles for the (2,2,0) configuration. The result from the analytical model in Eq. (1) is shown in black. The increase of the FWHM in (a) indicates the loss of interwire correlation, while in (b) it indicates a decreasing correlation length along the steps. At low temperatures the FWHM is constant in the $[\bar{3}\bar{3}10]$ direction up to ~ 90 K. Insets in (a),(b): Line profiles for both directions at various temperatures (shifted for better visibility). (c) Structural model of creation and separation of a soliton-antisoliton pair. Charge is transferred from an SDB to a UDB, generating a hop of the UDB to a neighboring site and creating a soliton-antisoliton pair. If this pair separates then a phase-shifted domain with $\times 3$ periodicity is formed.

were best fitted by a series of equidistant Lorentzian functions. No Gaussian-like central spike is found and the positions of the $\times 3$ diffraction spots do not shift with temperature. Across the steps, the full width at half maximum (FWHM) κ_{\perp} steadily increases as the temperature is raised from 60 to 130 K. Eventually, the spots merge into streaks, consistent with the vanishing of the $\times 3$ periodicity reported earlier [20].

Along the steps, the FWHM κ_{\parallel} is relatively constant up to about 100 K and then steadily increases as the temperature is raised further. This broadening of the $\times 3$ diffraction spots is due to increasing disorder in the arrangement of UDBs. This type of disorder originates from a simple microscopic process in which an electron [or two electrons, for the (2,2,0) configuration] hops from an SDB onto a neighboring UDB [middle panel of Fig. 3(c)]. As long as these electron hops do not bring neighboring UDBs closer than $2a_{\parallel}$, the configuration is metastable.

We used DFT to determine the formation energy E_0 of this elementary excitation, which can be viewed as a soliton-antisoliton bound pair. The calculations were performed in a 1×6 cell of Si(553)Au with four silicon double layers plus the reconstructed surface layer and a vacuum region of 10 \AA . All atomic positions were relaxed except the hydrogen-passivated bottom double layer. Total energies and forces were calculated using the generalized-gradient approximation of Perdew, Burke, and Ernzerhof (PBE) for the (2,2,1) configuration and the PBEsol revision of that functional for the (2,2,0) configuration, with projector-augmented wave potentials as implemented in VASP [38,41,42]. The plane-wave cutoff was 250 eV and the sampling of the surface Brillouin zone was 6×6 .

For the (2,2,1) ground-state configuration we find $E_0 = 30 \text{ meV}$, suggesting these defects will be numerous at temperatures above ~ 300 K, which is consistent with our experimental data. For the (2,2,0) configuration we find $E_0 = 85 \text{ meV}$, implying a much higher temperature scale of ~ 1000 K.

To investigate the concentration and distribution of defects as a function of temperature, we used the Metropolis Monte Carlo method to sample the steady-state arrangement of UDBs in an infinite array of dangling-bond wires with the Si(553)-Au geometry. We performed 10^7 trial hops at each temperature and computed the diffraction intensity from the positions of the UDBs. The spectra were convolved with a Gaussian to account for instrumental broadening in the experimental data. For the (2,2,1) configuration, the resulting FWHM of the $\times 3$ peaks is constant up to ~ 100 K and then increases gradually with temperature, in agreement with experiment but with smaller values [blue squares in Fig. 3(b)]. For the (2,2,0) configuration the FWHM is flat up to temperatures about $3 \times$ higher (blue triangles), as expected from the q^2 scaling of the Coulomb energy. See Supplemental Material [43] for additional details.

Even though the geometry of our model is 2D, the energy scale of Coulomb interactions across the wires is only 0.1 meV, 3 orders of magnitude smaller than E_0 . Hence, the interactions in the Monte Carlo simulations are essentially 1D. Our DFT calculations, however, reveal a much stronger interaction across the wires of order 1 meV. These may arise from the interaction of strain fields from the UDBs but other sources may contribute as well. Regardless of their origin, we turn now to investigating their role in the order-disorder transition. We show next that by including these 2D interactions, the FWHM at all temperatures is brought into quantitatively excellent agreement with experiment.

We constructed an exactly solvable Potts model Hamiltonian describing the dynamics of coupled wires and the resulting steady-state FWHM of the $\times 3$ peaks as a function of temperature:

$$\mathcal{H} = \sum_i [-b\delta_{u_i, u_{i+1}} - a\delta_{u_i, c}], \quad (1)$$

where $\delta_{i,j}$ denotes the Kronecker delta. A single UDB can take three positions within each unit cell i : left, center, and right, $u_i = \{l, c, r\}$. The first term, with parameter b , describes the energy needed to displace neighbouring UDBs relative to each other: specifically, the energy needed to create a soliton-antisoliton pair within one wire is $2b$. The second term, with parameter a , favors the occupation of the central position and arises from the coupling of the wire to neighboring wires. See Supplemental Material [43] for additional details.

The model fits best to our experimental data for $a = 2.1$ meV and $b = 21$ meV. These fitted values are also consistent with our DFT results: a should be equal to the calculated energy difference per UDB, 2.1 meV, between (2,2,1) configurations in staggered and centered alignments, and b corresponds to $E_0/2 = 15$ meV. In the Supplemental Material, we derive analytical expressions for the profiles and FWHM of the $\times 3$ peaks as a function of temperature [43]. The resulting FWHM, convolved as above with a Gaussian, is now in excellent agreement with our experimental results [black curve in Fig. 2(b)]. This improved agreement demonstrates that 2D coupling between neighboring wires indeed plays an important, central role in the order-disorder transition.

We turn now to the crossover from 2D to 1D behavior. At temperatures above ~ 120 K, the $\times 3$ diffraction spots are well described by a standard Lorentzian. At temperatures below ~ 90 K, the 2D character of the diffraction is more pronounced and hence the spot profiles are described by a Lorentzian to the power $3/2$ [44]. To characterize the transition between these two limits, we fit the spot profiles to a generalized Lorentzian,

$$\mathcal{L}(k_{\parallel}) = \frac{\Gamma(\nu)}{\sqrt{\pi}\Gamma(\nu - 1/2)} \frac{\kappa_{\parallel}^{2\nu-1}}{[(k_{\parallel} - k_0)^2 + \kappa_{\parallel}^2]^{\nu}}, \quad (2)$$

where k_{\parallel} is the reciprocal space coordinate in the $[1\bar{1}0]$ direction, k_0 is the position of the $\times 3$ diffraction spot, and

$\Gamma(x)$ is the Gamma function. The parameter $\nu = (d + 1)/2$ characterizes the dimensionality d of the system: $\nu = 3/2$ describes 2D systems while $\nu = 1$ describes 1D systems [44–46]; we constrained ν to lie in this range.

We find that ν exhibits a well-defined transition from 1.5 to 1.0 between $T_- = 93$ K and $T_+ = 128$ K (Fig. 4). The transition begins at about the temperature for which the FWHM κ_{\parallel} along the steps begins to increase [Fig. 2(b)]. Fitting the spot profiles without allowing ν to vary leads to significantly worse fits (insets to Fig. 4). The transition is completed at T_+ , where the FWHM κ_{\perp} across the wires exceeds the size of the surface Brillouin zone [Fig. 2(a)], reflecting the complete loss of long-range order across the wires. The underlying origin of this dimensional crossover is subtle but simple: the approximate geometrical isotropy of the 2D array of UDBs is broken by the strong anisotropy of the energy scales for creating disorder across and within the UDB wires. At temperatures above T_- soliton defects are still rare, but a rapidly growing fraction of the wire rows undergoes registry shifts with respect to each other and hence the 2D low-temperature state begins to behave like a collection of uncoupled 1D wires. As the temperature approaches T_+ this crossover becomes nearly complete. See the Supplemental Material [43] for additional discussion, modeling, and analysis.

To summarize, we have shown that silicon dangling-bond solitons in Si(553)-Au are created by thermal excitation. These defects interact via Coulomb forces within each step-edge atomic wire and via another mechanism, probably strain, across the wires. As the temperature is raised, the resulting disorder destroys the $\times 3$ positional long-range order of the UDBs within each wire and their registry across the wires. The nature of the interactions and their respective energy scales create a dimensional crossover of the

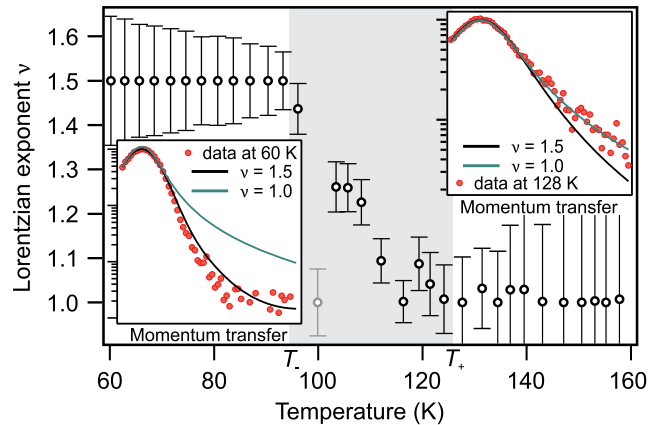


FIG. 4. Temperature dependence of the exponent ν of the generalized Lorentzian of Eq. (2) in the $[1\bar{1}0]$ direction. The exponent drops from 1.5 at $T_- = 93$ K to 1.0 at $T_+ = 128$ K, indicating a crossover from 2D to 1D behavior. Insets: Experimental and fitted spot profiles at 60 K and at T_+ . At 60 K the profile is best fit by $\nu = 3/2$ (2D behavior), while at T_+ the best fit is $\nu = 1$ (1D behavior).

order-disorder transition from 2D at low temperature to 1D at high temperature. The generality of this crossover can readily be investigated—both experimentally and using our theoretical methods—in other atomic wire systems in the Ge/Si(*hkk*)-Au family, where differences in the surface morphology and ground-state electron configuration may lead to further expanding our understanding of low-dimensional systems.

We acknowledge fruitful discussions with J. Aulbach, F. Hucht, J. König and J. Schäfer. This work was funded by the Deutsche Forschungsgemeinschaft (DFG, German Research Foundation)—Projektnummer 278162697—SFB 1242 and through Projektnummer 194370842—FOR1700. B. S. acknowledges financial support from the Ministry of Innovation NRW via the “Programm zur Förderung der Rückkehr des hochqualifizierten Forschungsnachwuchses aus dem Ausland.” This work was partly supported by the Office of Naval Research through the Naval Research Laboratory’s Basic Research Program (SCE). Computations were performed at the DoD Major Shared Resource Center at AFRL.

*Corresponding author.

bernd.hafke@uni-due.de

- [1] D. C. Tsui, H. L. Stormer, and A. C. Gossard, *Phys. Rev. Lett.* **48**, 1559 (1982).
- [2] R. B. Laughlin, *Phys. Rev. Lett.* **50**, 1395 (1983).
- [3] S.-i. Tomonaga, *Prog. Theor. Phys.* **5**, 544 (1950).
- [4] J. M. Luttinger, *J. Math. Phys. (N.Y.)* **4**, 1154 (1963).
- [5] M. Bockrath, D. H. Cobden, J. Lu, A. G. Rinzler, R. E. Smalley, L. Balents, and P. L. McEuen, *Nature (London)* **397**, 598 (1999).
- [6] J. R. Ahn, J. H. Byun, H. Koh, E. Rotenberg, S. D. Kevan, and H. W. Yeom, *Phys. Rev. Lett.* **93**, 106401 (2004).
- [7] T. Frigge, B. Hafke, T. Witte, B. Krenzer, C. Streubühr, A. Samad Syed, V. Mikšić Trontl, I. Avigo, P. Zhou, M. Ligges *et al.*, *Nature (London)* **544**, 207 (2017).
- [8] P. C. Snijders and H. H. Weitering, *Rev. Mod. Phys.* **82**, 307 (2010).
- [9] G. Grüner, *Rev. Mod. Phys.* **66**, 1 (1994).
- [10] A. Andrieux, D. Jérôme, and K. Bechgaard, *J. Phys. Lett.* **42**, 87 (1981).
- [11] K. Mortensen, *Solid State Commun.* **44**, 643 (1982).
- [12] Y. Sassa, M. Månsson, O. K. Forslund, O. Tjernberg, V. Pomjakushin, O. Ofer, E. J. Ansaldo, J. H. Brewer, I. Umegaki, Y. Higuchi *et al.*, *J. Electron Spectrosc. Relat. Phenom.* **224**, 79 (2018).
- [13] S. Dürrbeck, M. Hollerer, C. W. Thurner, J. Redinger, M. Sterrer, and E. Bertel, *Phys. Rev. B* **98**, 035436 (2018).
- [14] C. Brand, H. Pfnür, G. Landolt, S. Muff, J. H. Dil, T. Das, and C. Tegenkamp, *Nat. Commun.* **6**, 8118 (2015).
- [15] T. Das, *J. Phys. Condens. Matter* **28**, 294001 (2016).
- [16] C. Tegenkamp, Z. Kallassy, H. Pfnür, H.-L. Günter, V. Zielasek, and M. Henzler, *Phys. Rev. Lett.* **95**, 176804 (2005).
- [17] T. Block, C. Tegenkamp, J. Baringhaus, H. Pfnür, and T. Inaoka, *Phys. Rev. B* **84**, 205402 (2011).
- [18] M. J. Rice and E. J. Mele, *Phys. Rev. Lett.* **49**, 1455 (1982).
- [19] W. P. Su and J. R. Schrieffer, *Phys. Rev. Lett.* **46**, 738 (1981).
- [20] J. R. Ahn, P. G. Kang, K. D. Ryang, and H. W. Yeom, *Phys. Rev. Lett.* **95**, 196402 (2005).
- [21] J. N. Crain, A. Kirakosian, K. N. Altmann, C. Bromberger, S. C. Erwin, J. L. McChesney, J.-L. Lin, and F. J. Himpsel, *Phys. Rev. Lett.* **90**, 176805 (2003).
- [22] P. C. Snijders, S. Rogge, and H. H. Weitering, *Phys. Rev. Lett.* **96**, 076801 (2006).
- [23] J. S. Shin, K.-D. Ryang, and H. W. Yeom, *Phys. Rev. B* **85**, 073401 (2012).
- [24] I. Song, J. S. Goh, S.-H. Lee, S. W. Jung, J. S. Shin, H. Yamane, N. Kosugi, and H. W. Yeom, *ACS Nano* **9**, 10621 (2015).
- [25] J. Aulbach, J. Schäfer, S. C. Erwin, S. Meyer, C. Loho, J. Settelein, and R. Claessen, *Phys. Rev. Lett.* **111**, 137203 (2013).
- [26] S. Polei, P. C. Snijders, S. C. Erwin, F. J. Himpsel, K.-H. Meiwes-Broer, and I. Barke, *Phys. Rev. Lett.* **111**, 156801 (2013).
- [27] J. Aulbach, S. C. Erwin, J. Kemmer, M. Bode, J. Schäfer, and R. Claessen, *Phys. Rev. B* **96**, 081406(R) (2017).
- [28] B. Hafke, T. Frigge, T. Witte, B. Krenzer, J. Aulbach, J. Schäfer, R. Claessen, S. C. Erwin, and M. Horn-von Hoegen, *Phys. Rev. B* **94**, 161403(R) (2016).
- [29] L. Dudy, J. Aulbach, T. Wagner, J. Schäfer, and R. Claessen, *J. Phys. Condens. Matter* **29**, 433001 (2017).
- [30] H. W. Yeom, S. W. Jung, J. S. Shin, J. Kim, K. S. Kim, K. Miyamoto, T. Okuda, H. Namatame, A. Kimura, and M. Taniguchi, *New J. Phys.* **16**, 093030 (2014).
- [31] F. Edler, I. Miccoli, H. Pfnür, and C. Tegenkamp, *Phys. Rev. B* **100**, 045419 (2019).
- [32] J. Aulbach, S. C. Erwin, R. Claessen, and J. Schäfer, *Nano Lett.* **16**, 2698 (2016).
- [33] M. Krawiec, M. Kopciuszynski, and R. Zdyb, *Appl. Surf. Sci.* **373**, 26 (2016).
- [34] S. C. Erwin and F. J. Himpsel, *Nat. Commun.* **1**, 58 (2010).
- [35] M. Krawiec, *Phys. Rev. B* **81**, 115436 (2010).
- [36] J. P. Perdew, K. Burke, and M. Ernzerhof, *Phys. Rev. Lett.* **77**, 3865 (1996).
- [37] C. Braun, U. Gerstmann, and W. G. Schmidt, *Phys. Rev. B* **98**, 121402(R) (2018).
- [38] J. P. Perdew, A. Ruzsinszky, G. I. Csonka, O. A. Vydrov, G. E. Scuseria, L. A. Constantin, X. Zhou, and K. Burke, *Phys. Rev. Lett.* **100**, 136406 (2008).
- [39] P. Kury, R. Hild, D. Thien, H.-L. Günter, F.-J. Meyer zu Heringdorf, and M. Horn-von Hoegen, *Rev. Sci. Instrum.* **76**, 083906 (2005).
- [40] M. Krawiec and M. Jałochowski, *Phys. Rev. B* **87**, 075445 (2013).
- [41] G. Kresse and J. Hafner, *Phys. Rev. B* **47**, 558(R) (1993).
- [42] P. E. Blöchl, *Phys. Rev. B* **50**, 17953 (1994).
- [43] See Supplemental Material at <http://link.aps.org/supplemental/10.1103/PhysRevLett.124.016102> for a detailed description of the Monte Carlo simulations, the model Hamiltonian, and the modeling of the dimensional crossover.
- [44] J. Wollschläger, E. Z. Luo, and M. Henzler, *Phys. Rev. B* **44**, 13031 (1991).
- [45] C. S. Lent and P. I. Cohen, *Surf. Sci.* **139**, 121 (1984).
- [46] P. R. Pukite, C. S. Lent, and P. I. Cohen, *Surf. Sci.* **161**, 39 (1985).